

Incoherent Holographic Interferometry

Kaige Wang

*Department of Physics, Applied Optics Beijing Area Major
Laboratory, Beijing Normal University, Beijing
China*

1. Introduction

The original meaning of coherence was attributed to the ability of light to exhibit interference phenomena. There are two types of coherence: temporal coherence and spatial coherence. Temporal coherence measures the ability of two relatively delayed beams to form interference fringe. Interference in a Michelson interferometer refers to temporal coherence. However, spatial coherence reflects the ability of a beam to interfere with a spatially shifted (but not delayed) version across the beam. Young's double-slit experiment is an example which concerns spatial coherence.

Since the first experimental realization of Young's double-slit interference, it has been known that the observation of interference-diffraction pattern of an object requires a spatially coherent source. The waves emitted from positions outside the coherent area possess independent irregular phases which may degrade the interference pattern. In the early days when coherent sources were unavailable, interference experiments were carried out with an extended thermal source restricted by a pinhole aperture, which can improve the spatial coherence. Holography is one of the most important applications of spatial interference. In the first holography experiment, Dennis Gabor stated that (Gabor, 1972) "The best compromise between coherence and intensity was offered by the high-pressure mercury lamp, which had a coherence length of only 0.1 millimeter, ... But in order to achieve spatial coherence, we had to illuminate, with one mercury line, a pinhole 3 microns in diameter. " The pinhole eventually reduced the power of the source and thus impeded the potential application of optical interferometric techniques such as holography. This barrier was overcome with the invention of the laser, whose intense and coherent beam was ideal for performing interference.

Coherent sources are obtainable within a certain range of optical frequencies. However, various holographic techniques have been developed using incoherent sources such as X-rays, electrons, and γ radiation. To improve the coherence one has to pay the cost of decreasing the intensity of the source, as already pointed out in relation to Gabor's experiment. A challenging question would be whether coherence is absolutely necessary in holography, or can we bypass the coherence requirement? As a matter of fact, in the early days of holography, a technique using incoherent illumination was first proposed by Mertz and Young (Mertz & Young, 1963), and then extended by Lohmann (Lohmann, 1965), Stroke and Restrick (Stroke & Restrick, 1965), and Cochran (Cochran, 1966). The strategy is based on the fact that each point of a spatially incoherent object produces, through interference of

its wave fronts, a stationary interference pattern which uniquely encodes the position and intensity of the object point. However, the method has various weaknesses that significantly limit its application. The schemes proposed for incoherent holography can only record the intensity distribution of a fluorescent object. Moreover, each elementary fringe pattern is formed by two extremely tiny portions of the light, and the summation of many weak interference patterns results in a very large bias level in the hologram, much larger than that in coherent holography. Hence incoherent holography is appropriate only for objects with a low number of resolution elements (Goodman, 1996).

In this chapter we introduce an incoherent interference mechanism which seems to contradict our existing knowledge of the interference requirements. Consider a holographic interferometer in which an object is placed in one arm; the object wave then interferes with the reference wave in the other arm, resulting in an interference pattern which records the object information. To obtain well-defined interference fringes in an ordinary balanced interferometer where both arms have the same path length, the optical field illuminating the interferometer must have spatial coherence, that is, its transverse coherence length must be large enough. We find that the requirement of spatial coherence is due to the particular geometry of the balanced interferometer. If the two fields to be interfered travel through different lengths or different diffraction configurations, then spatial coherence is no longer necessary for spatial interference. Thus we have proposed several unbalanced interferometers where the two beams travel different path lengths or have different diffraction configurations (Zhang et al., 2009a, 2009b). These interferometers are capable of exhibiting interference using either coherent or spatially incoherent light, but their interference fringes are different, signifying that they have different origins.

The chapter is organized as follows. In Section 2 we first analyze why both temporal and spatial coherence conditions are necessary in an ordinary holographic interferometer. Then we propose an unbalanced holographic interferometer with different path lengths and demonstrate that it can exhibit interference using a light source with spatial incoherence. The setup is capable of performing holography. In Section 3 we further suggest several types of unbalanced interferometers which are able to realize incoherent interferometry. In particular, some of the schemes can reduce the requirement of temporal coherence and employ a true incoherent source such as a lamp with an extended illumination area. Moreover, we show that phase reversal diffraction can occur in the incoherent interferometer. Finally, a brief summary is given in Section 4.

2. What is incoherent interferometry?

We consider a holographic interferometer as shown in Fig. 1, in which an object field $E_o(x)$ and a reference field $E_r(x)$ are reflected from mirrors M_1 and M_2 , respectively, to interfere at the recording plane RP. The intensity distribution of their superposed field is written as

$$I(x) = \langle |E_o(x) + E_r(x)|^2 \rangle = \langle |E_o(x)|^2 \rangle + \langle |E_r(x)|^2 \rangle + \{ \langle E_r^*(x)E_o(x) \rangle + c.c. \}, \quad (1)$$

where x is the transverse coordinate across the beam, and $\langle E_r^*(x)E_o(x) \rangle$ the interference term. In the interferometric scheme the two fields must come from the same source field $E_s(x)$. Let a transmitting object O with transmittance $T(x)$ be close to the source, so the two fields can be expressed as

$$E_o(x, t) = \int T(x_1) h_o(x, x_1) E_s(x_1, t_1) dx_1, \quad (2a)$$

$$E_r(x, t) = \int h_r(x, x_2) E_s(x_2, t_2) dx_2, \quad (2b)$$

where $h_o(x, x_1)$ and $h_r(x, x_2)$ are the impulse response functions for the object and reference paths, t_1 and t_2 are the times taken for the source fields to propagate to the recording plane through the object and reference paths, respectively. x_j ($j = 1, 2$) is the transverse coordinate in the source field. Hence the interference term is obtained to be

$$\langle E_r^*(x, t) E_o(x, t) \rangle = \int T(x_1) h_o(x, x_1) h_r^*(x, x_2) \langle E_s^*(x_2, t_2) E_s(x_1, t_1) \rangle dx_1 dx_2. \quad (3)$$

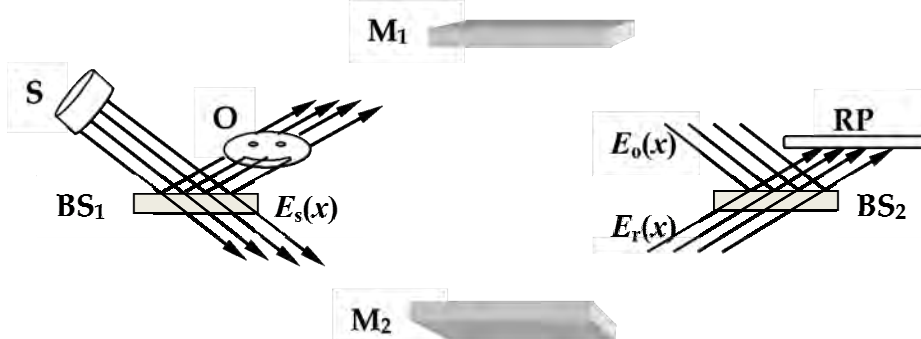


Fig. 1. A holographic interferometer consisting of two beam splitters, BS_1 and BS_2 , and two mirrors, M_1 and M_2 ; S is a source and O an object; RP is the recording plane.

The temporal coherence of the source field is characterized by the coherence time τ . If $|t_2 - t_1|$ is larger than τ , then $\langle E_s^*(x_2, t_2) E_s(x_1, t_1) \rangle = 0$ and interference never occurs. However, spatial coherence requires that the beam has a well-defined wave-front, such as a field emitted from a point source or a laser beam. When the source field satisfies both temporal and spatial coherence, then

$$\langle E_s^*(x_2, t_2) E_s(x_1, t_1) \rangle = E_s^*(x_2, t_2) E_s(x_1, t_1). \quad (4)$$

Thus coherent interferometry occurs in the form of

$$\langle E_r^*(x, t) E_o(x, t) \rangle = E_r^*(x, t) E_o(x, t), \quad (5)$$

which contains the object information. This is what has been known before.

We now consider the case when the source field satisfies temporal coherence (i.e. $|t_2 - t_1| < \tau$) but not spatial coherence. The first-order correlation function of the source field is written as

$$\langle E_s^*(x_2, t_2) E_s(x_1, t_1) \rangle = I_s e^{i\varphi} \delta(x_2 - x_1), \quad (6)$$

where φ is an arbitrary phase. For simplicity, the intensity distribution I_s is assumed to be homogeneous. Equation (6) describes complete spatial incoherence. The wave-front of the beam fluctuates randomly and any two positions across the beam are statistically independent. Substituting Eq. (6) into Eq. (3), we obtain

$$\langle E_r^*(x) E_o(x) \rangle = I_s e^{i\varphi} \int T(x_0) h_o(x, x_0) h_r^*(x, x_0) dx_0. \quad (7)$$

For a conventional balanced interferometer where the two optical paths have the same length, that is $h_o(x, x_0) = h_r(x, x_0)$, then $h_o(x, x_0)h_r^*(x, x_0)$ is x -independent. In the paraxial approximation, for example, the impulse response function for a propagation length z is given by

$$\begin{aligned} H(x, x_0; z) &= \sqrt{\frac{k}{i2\pi z}} \exp(ikz) \exp\left[\frac{ik(x-x_0)^2}{2z}\right] \\ &= \sqrt{\frac{k}{i2\pi z}} \exp(ikz) G(x - x_0, z), \end{aligned} \quad (8a)$$

$$G(x, z) \equiv \exp\left[\frac{ikx^2}{2z}\right], \quad (8b)$$

where k is the wave number, so $H(x, x_0; z)H^*(x, x_0; z) = k/(2\pi z)$ is x -independent. Therefore, the interference term (7) yields

$$\langle E_r^*(x)E_o(x) \rangle \propto \int T(x_0)dx_0, \quad (9)$$

and the object information has been washed out. We can also prove that, no matter where the object is placed within the object path, Eq. (9) still holds provided the two paths of the interferometer have the same length. Perhaps this consequence brought about the misunderstanding that spatial interference in holography needs not only temporal but also spatial coherence. The following experiment will show that the condition of spatial coherence is not necessary if the interferometric scheme is modified.

In 2009 we proposed an incoherent interferometry setup as shown in Fig. 2 (Zhang et al., 2009a). In this unbalanced interferometer the object and reference arms have different lengths, $z_o = 16\text{cm}$ and $z_r = 27\text{cm}$, respectively. The spatially incoherent light source is formed by passing a He-Ne laser beam of wavelength 632.8nm through a rotating ground glass disk. The object in the experiment is a double slit T of slit width $b = 125\mu\text{m}$ and spacing $d = 310\mu\text{m}$. The interference pattern can be recorded by either of two charge-coupled device (CCD) cameras.

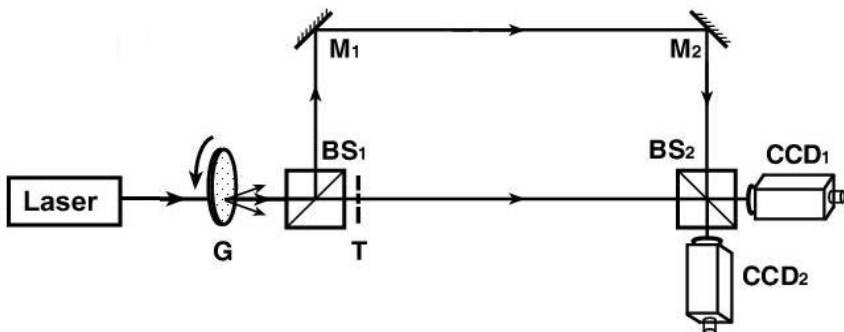


Fig. 2. Experimental scheme for an unbalanced interferometer where the two arms have different lengths. A laser and a rotating ground glass disk G form a spatially incoherent source; M_1 and M_2 are mirrors, BS_1 and BS_2 are beamsplitters, CCD_1 and CCD_2 are detectors, and T is a double-slit close to BS_1 .

The laser beam has good temporal coherence which will not be affected by the scattering of the slowly rotating ground glass. The path difference between the two arms is much smaller than the longitudinal coherence length $c\tau$, where c is the light speed in vacuum and τ is the coherence time of the laser beam. However, the motion of the ground glass disk destroys the spatial coherence of the laser beam. This source emits what is known as pseudo-thermal light and satisfies Eq. (6) approximately. In contrast, a true thermal light source cannot satisfy the condition of temporal coherence in this setup.

The two-dimensional (2D) intensity patterns detected by CCD_1 are shown in Fig. 3. When the ground glass disk is moved step by step, the interference patterns are irregular speckles frame by frame and each frame is different, as shown in the two single-shot frames of Figs. 3(a) and 3(b). However, if we average over a number of exposures, as the number of frames increases, a well-defined interference pattern emerges gradually, as can be seen in Figs. 3(c)-3(g).

The experimental results tell us that, unlike the stationary pattern in coherent interferometry, the interference pattern here is irregularly fluctuating in time and the well-defined pattern can only be discerned after taking its statistical average. These striking features imply that incoherent interferometry originates from a different interference mechanism.

We can explain the experiment using Eq. (7). The interference term in this incoherent interferometer can be calculated as

$$\begin{aligned} \langle E_r^*(x)E_o(x) \rangle &= I_s e^{ik\phi} \int T(x_0)H(x, x_0; z_0)H^*(x, x_0; z_r)dx_0 \\ &\propto \exp[ik(z_0 - z_r)] \int T(x_0)G(x - x_0, z_0)G^*(x - x_0, z_r)dx_0 \\ &= \exp[ik(z_0 - z_r)] \int T(x_0)G(x - x_0, Z)dx_0, \end{aligned} \quad (10)$$

where function G defined by Eq. (8b) obeys

$$G(x, z_0)G^*(x, z_r) = G(x, Z), \quad (11)$$

when the effective diffraction length Z is defined by

$$\frac{1}{Z} = \frac{1}{z_0} - \frac{1}{z_r}. \quad (12)$$

Equation (10) defines a kind of incoherent interferometry, which represents the Fresnel diffraction integral of an object under the paraxial condition, and is the same as for coherent diffraction but with an effective object distance Z replacing the real one, z_0 . Note that Z is negative for $z_0 > z_r$, designating a phase reversal diffraction. We will discuss this issue in Subsection 3.3.

In the far-field limit, Eq. (10) presents the Fourier transform \tilde{T} of object T :

$$\langle E_r^*(x)E_o(x) \rangle \propto \exp[ik(z_0 - z_r)] G(x, Z) \tilde{T}\left(\frac{kx}{Z}\right). \quad (13)$$

For a double-slit of slit width b and spacing d , its Fourier transform reads

$$\tilde{T}(q) = \left(\frac{2b}{\sqrt{2\pi}}\right) \text{sinc}(qb/2) \cos(qd/2). \quad (14)$$

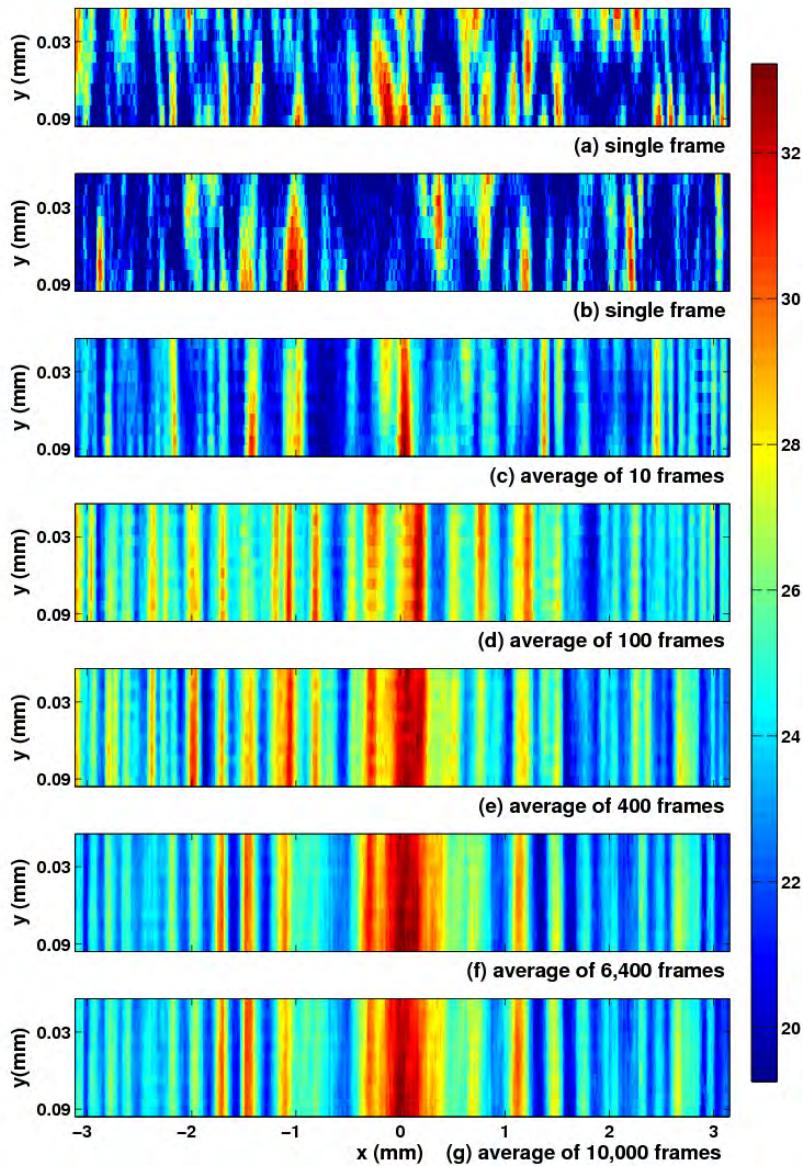


Fig. 3. Experimentally observed 2D interference patterns recorded by CCD1 in the scheme of Fig. 2. Figs. (a) and (b) are individual single frames; (c), (d), (e), (f) and (g) are averaged over 10, 40, 400, 6400 and 10000 frames, respectively. The color-bar shows the relative intensity.

Besides the interference term, however, the output intensity distribution of the interferometer includes also the intensities of both the object and reference waves [see Eq. (1)]. In incoherent interferometry, these two intensities are homogeneously distributed.

In contrast, for the same interferometer driven by coherent light, Eq. (5) yields

$$\begin{aligned}\langle E_r^*(x)E_o(x) \rangle &\propto \exp[ik(z_o - z_r)] \int T(x_0)G(x - x_0, z_o)dx_0 \\ &\approx \exp[ik(z_o - z_r)] G(x, z_o) \tilde{T}\left(\frac{kx}{z_o}\right),\end{aligned}\quad (15)$$

where the last step is valid in the far-field limit. However, the intensity distribution of the reference waves is homogeneous whereas the intensity of the object wave exhibits the diffraction pattern

$$\langle |E_o(x)|^2 \rangle \propto |\int T(x_0)G(x - x_0, z_o)dx_0|^2 \approx \left| \tilde{T}\left(\frac{kx}{z_o}\right) \right|^2. \quad (16)$$

In holography this pattern should be avoided by diminishing the intensity of the object wave.

To demonstrate the above theoretical explanation, Fig. 4 shows one-dimensional (1D) intensity patterns recorded by the two CCD cameras, where (a) and (b) are the interference fringes observed by CCD_1 and CCD_2 , respectively. The left part shows the results when the interferometer is illuminated by spatially incoherent light. In our experimental scheme the effective diffraction length is calculated to be $Z = 39.3\text{cm}$. For a 50/50 beamsplitter BS_2 , if one output field is $[E_r(x) + E_o(x)]/\sqrt{2}$, the other should be $[E_r(x) - E_o(x)]/\sqrt{2}$. We can see that the two interference patterns with a phase shift π are formed in the average of 10000 frames, which matches with the theoretical simulation of Eq. (13). Taking the difference and sum of the two output intensities gives, respectively, the net interference pattern and the intensity background, as shown in (c) and (d). As a matter of fact, the homogeneous intensity background verifies the spatial incoherence of the source.

To further confirm whether the interference pattern is related to the spatial incoherence, we compare it with the result obtained in the same interferometer using coherent light. For this we simply remove the ground glass disk in Fig. 2. The experimental results and theoretical simulation are shown in the right part of Fig. 4, where (a) and (b) show the stationary intensity patterns registered by CCD_1 and CCD_2 , respectively. In the coherent case, these patterns contain the interference term and the diffraction pattern of the object. Again, taking the difference and sum of (a) and (b), we obtain the net interference pattern in (c) and the diffraction pattern of the object in (d), respectively. These experimental results are very different from the left part for incoherent interferometry, and agree well with Eqs. (15) and (16) with a diffraction length of $z_o = 16\text{cm}$ for the coherent case.

The above theoretical analysis and experimental demonstration tell us that, in an unbalanced interferometer, spatially incoherent light is capable of performing holographic interference in a similar way to that of coherent light. When an object is illuminated by incoherent light, the coherent information is lost in the object wave itself, but can be reproduced in an unbalanced interferometric scheme. Physically, the mechanisms of the two types of interferometry are quite different. In the incoherent case, the interference pattern fluctuates irregularly in time, and a well-defined pattern can only be formed in the statistical summation. Moreover, the diffraction pattern of an object is dependent on the effective diffraction length, which is associated with the travel distances of both the object and reference waves.

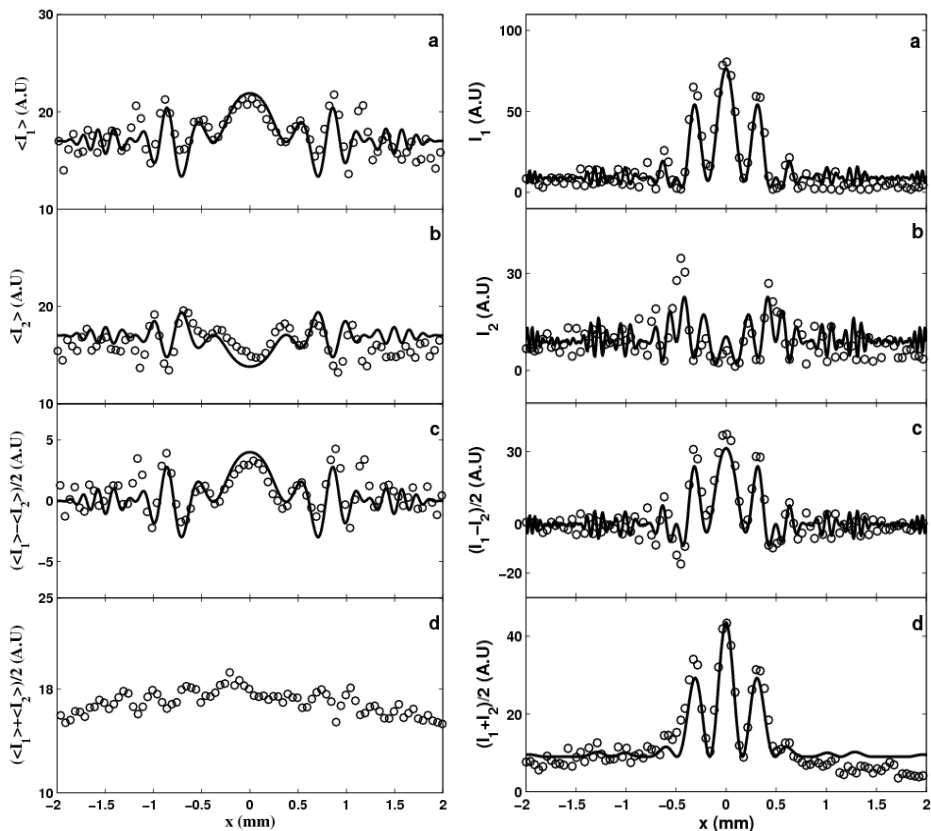


Fig. 4. Experimentally observed 1D interference patterns in the scheme of Fig. 2. Left and right parts are the patterns obtained using spatially incoherent and coherent light, respectively. (a) and (b) are the patterns registered by CCD_1 and CCD_2 , respectively; (c) and (d) are their difference and summation, respectively. The patterns for the incoherent case are averaged over 10000 frames. Experimental data and theoretical simulation are given by open circles and solid lines, respectively.

3. Various schemes for incoherent interferometry

In the last section, we indicated that incoherent interferometry does not exist in a balanced interferometer and we proposed an unbalanced interferometer where its two arms have different lengths. Based on this attribute, in this section, we propose other unbalanced interferometers to perform incoherent interference.

3.1 Scheme I

As shown in Fig. 5, we modify the previous interferometer by inserting two lenses in the centre of the two arms (Zhang, July 2010). Since a lens can perform Fourier transformation

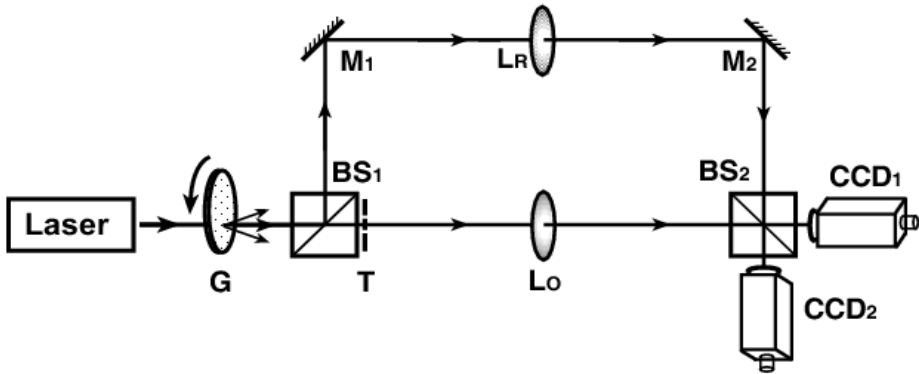


Fig. 5. Scheme I of incoherent interferometry, which is similar to the scheme of Fig. 2 but two lenses are inserted in the centre of the two arms. Both the input and output ports of the interferometer are located at the two focal planes of the lenses.

of a field between its two focal planes, we position both the input and output ports of the interferometer at the two foci of the lenses. The impulse response function between the two focal planes for a lens of focal length f is given by

$$h(x, x_0) = F(x, x_0; f) \equiv \sqrt{k/(i2\pi f)} \exp(i2kf) \exp(-ikxx_0/f), \quad (17)$$

where k is the wave number of the beam.

Let object $T(x_0)$ be close to the input port. In the incoherent regime, then Eq. (7) gives the interference term to be

$$\begin{aligned} \langle E_r^*(x) E_o(x) \rangle &\propto \int T(x_0) F(x, x_0; f_o) F^*(x, x_0; f_r) dx_0 \\ &\propto \exp[i2k(f_o - f_r)] \int T(x_0) \exp[-ikxx_0/f] dx_0 \\ &= \exp[i2k(f_o - f_r)] \tilde{T}[kx/f], \end{aligned} \quad (18)$$

where f_o and f_r are the focal lengths of the lenses in the object arm and reference arm, respectively. The effective focal length f is defined as

$$\frac{1}{f} = \frac{1}{f_o} - \frac{1}{f_r}. \quad (19)$$

In the experiment we take the two lenses to be of focal lengths $f_o = 7.5\text{cm}$ and $f_r = 12\text{cm}$, and the double-slit as the object. The experimental results are plotted in Fig. 6. After eliminating the background, Fig. 6(c) shows the Fourier spatial spectrum of the double-slit. The theoretical curves are plotted by using Eqs. (18) and (19) with the effective focal length $f = 20\text{cm}$.

If a coherent plane wave drives the same interferometer, the interference term is obtained as

$$\langle E_r^*(x) E_o(x) \rangle \propto \exp[i2k(f_o - f_r)] \tilde{T}[kx/f_o] \delta(x), \quad (20)$$

where Dirac Delta function $\delta(x)$ comes from the focusing effect of the lens in the reference wave, and the Fourier transform of the object is governed by the focal length f_o of the object

lens. However, this Fourier spectrum will not appear in the coherent interference term due to the modulation of Delta function.

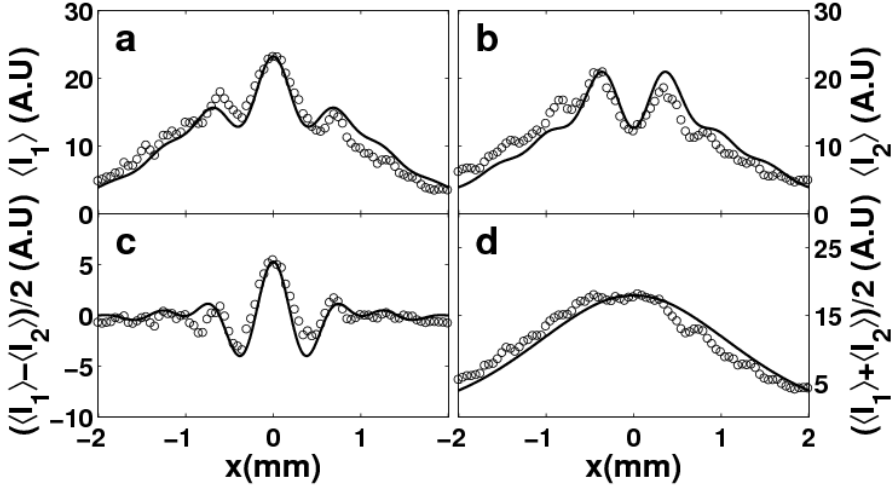


Fig. 6. Experimentally observed 1D interference patterns in Scheme I (Fig. 5). (a) and (b) are interference patterns (averaged over 10000 frames) registered by CCD_1 and CCD_2 , respectively; (c) and (d) are their difference and summation, respectively. Experimental data and theoretical simulation are given by open circles and solid lines, respectively.

3.2 Scheme II

In the previous interferometric schemes, the two arms have different optical path lengths so they require the light source to have much better temporal coherence, which is possible only by using a laser beam. A quasi-monochromatic thermal light source with an extended area can be regarded as a spatially incoherent source with a short coherence time less than 0.1 nsec. Therefore a true thermal light source fails in these schemes. From an application point of view, we must look for other schemes if we wish to employ a true thermal light source. For this purpose, the two arms of the interferometer must have equal optical path lengths but different diffraction configurations. We propose the following schemes for a true thermal light source.

We first consider an interferometer in which the two arms have the same length, $2f_0$ (Zhang et al. 2009a). As shown in Fig. 7, a lens L_o of focal length $f_0 = 19\text{cm}$ is set in the centre of the object arm, while in the other arm the beam travels freely to beamsplitter BS_2 . Hence the diffraction through the lens in the object arm has a different configuration from that for free propagation in the other arm.

Let object $T(x)$ and the CCD cameras be placed at the two focal planes of lens L_o , which produces the Fourier transform of the object. In the coherent regime, the interference term given by Eq. (5) exhibits the Fourier spatial spectrum of the object $T(x)$

$$\langle E_r^*(x)E_o(x) \rangle \propto \tilde{T}(kx/f_0). \quad (21)$$

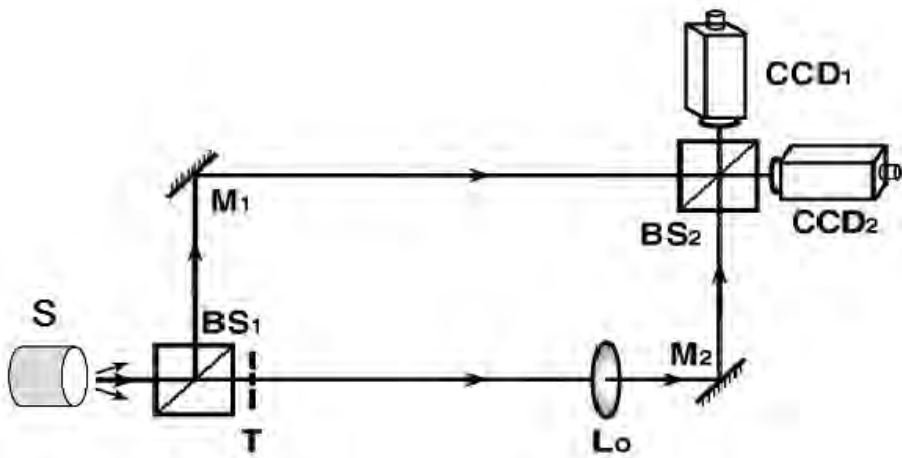


Fig. 7. Scheme II of incoherent interferometry, where S is a light source. A lens L_o of focal length f_o is set in the centre of the object arm, and both arms have the same length $2f_o$.

However, in the incoherent regime, Eq. (7) gives the interference term to be

$$\begin{aligned} \langle E_r^*(x)E_o(x) \rangle &\propto \int T(x_0)F(x, x_0; f_o)H^*(x, x_0; 2f_o)dx_0 \\ &\propto \int T(x_0)G^*(x + x_0, 2f_o)dx_0 \\ &\approx G^*(x, 2f_o)\tilde{T}\left[\frac{kx}{2f_o}\right], \end{aligned} \quad (22)$$

where the last step is valid in the far-field limit. The equation shows the Fresnel diffraction pattern of the object with a diffraction length $2f_o$, different from the f_o in Eq. (21).

With the above experimental scheme, we have used four types of sources. Figure 8 shows 1D patterns using the same sources as in the scheme of Fig. 2; the left part corresponds to a He-Ne laser beam passing through a ground glass plate while the right part, the direct laser beam. We can see that the interference patterns in the left part are very similar to those in Fig. 4. As a matter of fact, these two incoherent interferometry schemes exhibit similar Fresnel diffraction with slightly different effective diffraction lengths, $Z = 39.3\text{cm}$ and $2f_o = 38\text{cm}$. When the ground glass plate is removed, coherent interference patterns are registered by CCD_1 and CCD_2 , as shown in the right part of Figs. 8(a) and 8(b), respectively. They are the spatial Fourier spectra of the double-slit, consisting of two parts, $\tilde{T}(kx/f_o) + c.c.$ and $|\tilde{T}(kx/f_o)|^2$. The former and the latter can be extracted by the difference and sum of (a) and (b), as shown in the right part of Figs. 8(c) and 8(d), respectively.

As the third source we use a Na lamp emitting true thermal light of wavelength 589.3 nm , with an illumination area of $10 \times 10 \text{ mm}^2$, to replace the previous source in Fig. 2. In this case, the interference pattern directly appears on the CCD screen and it is not necessary to perform statistical averaging, as shown in Fig. 9(b). This is due to the fact that the response time of the CCD camera is much longer than the time scale of the thermal light fluctuations, so that averaging has already taken place in a single exposure. For comparison, Fig. 9(a)

shows the 2D interference pattern corresponding to Fig. 8(a, left) for pseudo-thermal light. The two sets of fringes are similar, but have slightly different spacings, due to the different wavelengths of the two sources. Finally, we set a pinhole of diameter 0.36 mm after the lamp to dispel the spatial incoherence. With this point-like source, a different interference pattern, which has half the fringe spacing of that for the spatially incoherent source, appears on the CCD screen, as shown in Fig. 9(c). Consequently, the present scheme is favorable for realizing incoherent interferometry using a true incoherent source.

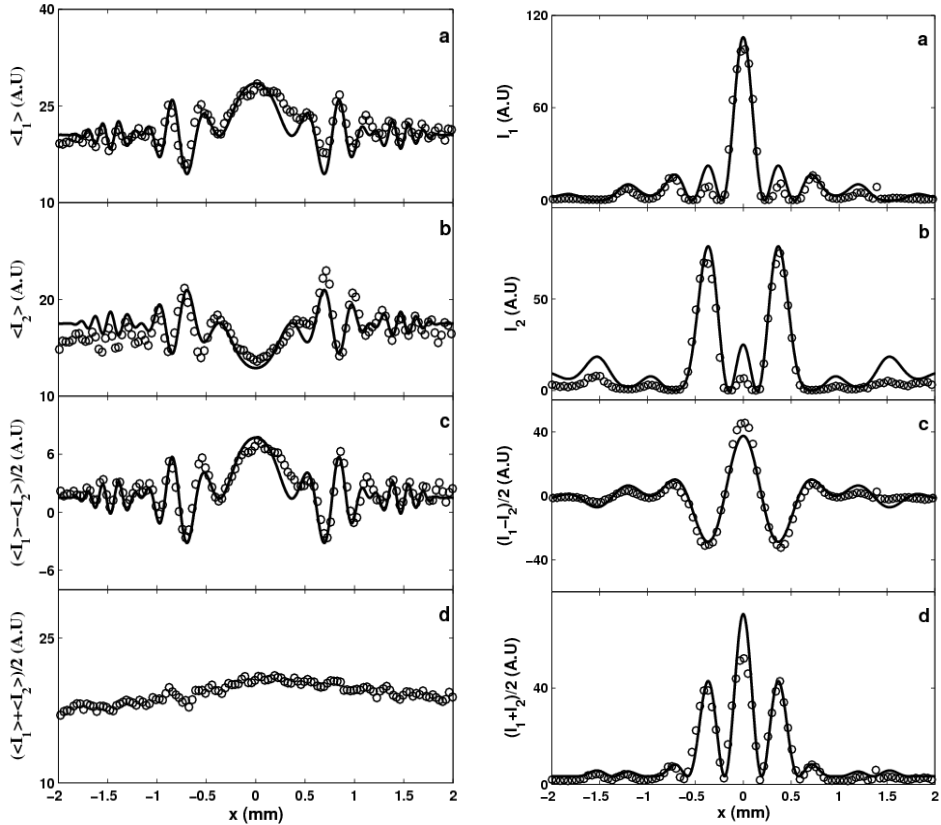


Fig. 8. Experimentally observed 1D interference patterns in the scheme of Fig. 7. Left and right parts are the patterns using spatially incoherent and coherent light, respectively. (a) and (b) are interference patterns (averaged over 10000 frames) registered by CCD_1 and CCD_2 , while (c) and (d) are their difference and summation, respectively. Experimental data are given by open circles and theoretical simulation by solid lines.

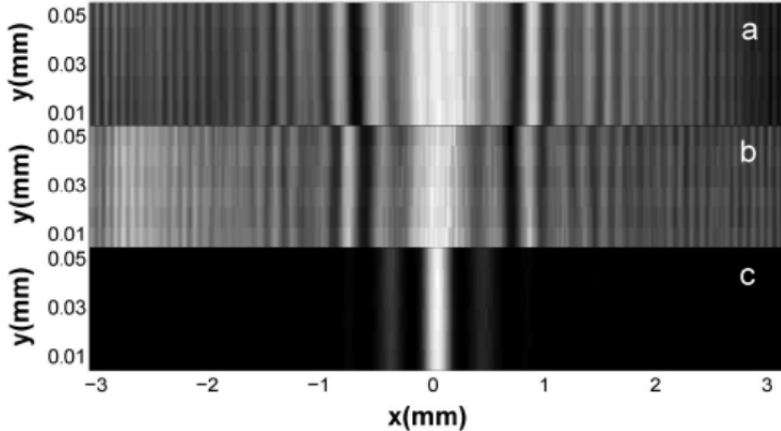


Fig. 9. Experimentally observed 2D interference patterns registered by CCD_1 in the scheme of Fig. 7: (a) with the original pseudo-thermal light source in Fig. 2, averaged over 10000 frames; (b) with a Na lamp of extended illumination area as the light source; (c) with a Na lamp followed by a pinhole as the light source. (Zhang et al., 2009a)

3.3 Scheme III

In this subsection we propose an interesting interferometric scheme which displays unusual behavior in incoherent interferometry. The setup is a simple modification of Fig. 2 whereby a transparent glass rod is inserted into one arm (Zhang et al. 2009b). The length of the rod is selected in such a way that the two arms of the interferometer have equal optical path lengths although their physical lengths are different. Thus the interferometer does not require the driving beam to have better temporal coherence.

The rod can also upset the balanced diffraction between the two arms. When a wave travels over a distance z in a homogeneous material of refractive index n , the impulse response function is given by

$$h(x, x_0) = \sqrt{\frac{k_0}{i2\pi(z/n)}} \exp[ik_0(nz)] \exp\left[\frac{i(k_0(x-x_0))^2}{2(z/n)}\right], \quad (23)$$

where k_0 is the wave number in vacuum. It should be noted that in the glass rod medium the optical path length nz is different from the diffraction length z/n . We rewrite Eq. (23) in the form of

$$H(x, x_0; nz, z/n) = \sqrt{\frac{k_0}{i2\pi(z/n)}} \exp(ik_0 nz) G(x - x_0, z/n), \quad (24)$$

where n_z and z/n are the optical path and diffraction lengths of the rod, respectively. In successive free propagation through two regions of optical path length z_j and diffraction length \bar{z}_j ($j = 1, 2$), we obtain the impulse response function of the combined diffraction to be

$$H(x, x_0; z_1 + z_2, \bar{z}_1 + \bar{z}_2) = \int H(x, x'; z_1, \bar{z}_1)H(x', x_0; z_2, \bar{z}_2)dx'. \quad (25)$$

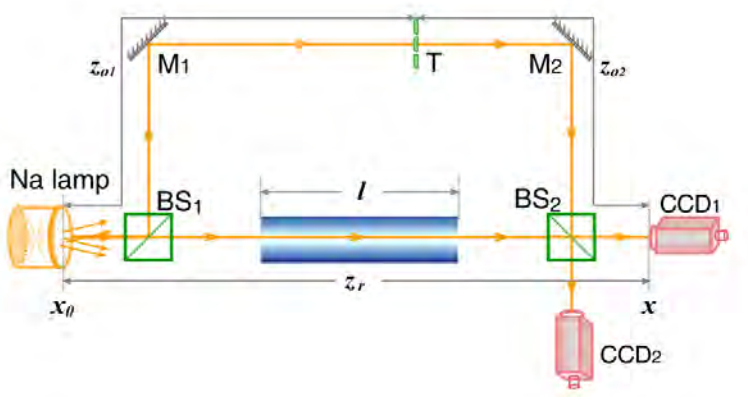


Fig. 10. Scheme III of incoherent interferometry, which is similar to the scheme of Fig. 2 but a glass rod is placed in one arm. The two ends of the rod are plane. (Zhang et al., 2009b)

In general, for a series of cascaded media, the impulse response function $H(x, x_1; Z, \bar{Z})$ corresponds to an optical path length $Z = n_1 l_1 + n_2 l_2 + \dots$, and a diffraction length $\bar{Z} = \frac{l_1}{n_1} + \frac{l_2}{n_2} + \dots$. As an example, we calculate the impulse response function of the reference arm in the present interferometer. The physical length of the reference arm is z_r while the glass rod is of length l and refractive index n . We thus require the impulse response function $H(x, x_0; Z, \bar{Z})$ for an optical path length of $Z = z_r - l + nl$ and diffraction length $\bar{Z} = z_r - l + l/n$.

In the other arm, object $T(x)$ is placed at the position which is at a distance z_{o1} from the source and z_{o2} from either of the CCD cameras. The impulse response function is written as

$$h_o(x, x_0) = \int H(x, x'; z_{o2}, z_{o2})T(x')H(x', x_0; z_{o1}, z_{o1})dx'. \quad (26)$$

According to Eq. (7), the interference term can be calculated to be

$$\begin{aligned} \langle E_r^*(x)E_o(x) \rangle &\propto \int H^*(x, x_0; Z, \bar{Z})H(x, x'; z_{o2}, z_{o2})T(x')H(x', x_0; z_{o1}, z_{o1})dx'dx_0 \\ &= \int H(x, x'; z_{o1} - Z, z_{o1} - \bar{Z})H(x, x'; z_{o2}, z_{o2})T(x')dx' \\ &\propto \exp[ik_0(z_o - Z)] \int T(x')G(x - x', Z_{\text{eff}})dx', \end{aligned} \quad (27)$$

where the Gaussian function G has been defined by Eq. (8b), $z_o = z_{o1} + z_{o2}$ is the length of the object arm, and the effective diffraction length Z_{eff} is defined by

$$\frac{1}{Z_{\text{eff}}} = \frac{1}{z_{o2}} + \frac{1}{z_{o1} - \bar{Z}}. \quad (28)$$

As a result, Eq. (27) represents Fresnel diffraction with the effective diffraction length Z_{eff} . The equal-optical-path condition of the interferometer is thus

$$z_o = Z = z_r + (n - 1)l. \quad (29)$$

Under this condition, the effective diffraction length becomes

$$Z_{\text{eff}} = z_{o2} \left[1 - \frac{z_{o2}}{l(n - \frac{1}{n})} \right]. \quad (30)$$

As long as a certain length l of a medium with index $n \neq 1$ satisfies Eq. (29), the interferometer is capable of realizing incoherent interferometry with a true incoherent light source. The effective diffraction length can be positive or negative, corresponding to normal or phase reversal diffraction, respectively.

In particular, when an object is located at the position $z_{o2}|_{\text{img}} = l(n - \frac{1}{n})$, the effective diffraction length is zero, i.e., $Z_{\text{eff}} = 0$. It turns out that $G(x - x', Z_{\text{eff}} = 0) \propto \delta(x - x')$ in Eq. (27). This means that the wave-front of a beam can be exactly recovered in the propagation. In other words, the image of the object is reproduced with an equal size on the CCD screen. Equation (30) is rewritten as

$$Z_{\text{eff}} = z_{o2} \left[1 - \frac{z_{o2}}{z_{o2}|_{\text{img}}} \right]. \quad (31)$$

Moreover, the distance of the object from the source for imaging to be obtainable is given by

$$z_{o1}|_{\text{img}} = z_o - z_{o2}|_{\text{img}} = z_r - l + \frac{l}{n} = \bar{Z}. \quad (32)$$

Thus this distance can be evaluated from the diffraction length of the reference arm.

In the experimental scheme of Fig. 10, the object and reference arms have lengths of $z_o = 41.8$ cm and $z_r = 33.8$ cm, respectively. When the length of the glass rod of refractive index $n=1.5163$ is $l = 15.5$ cm, the optical path of the reference arm is equal to that for the object arm, i.e. $Z = z_o = 41.8$ cm, although their physical lengths are different. Under this equal-optical-path condition, the two fields to be interfered at the detection plane come from the same wave-front of the source, hence we may use illumination from an incoherent thermal light source, such as the Na lamp mentioned above. Moreover, the diffraction length of the reference arm can be calculated to be $\bar{Z} = z_r - l + \frac{l}{n} = 28.5$ cm, so the imaging position in the object arm is $z_{o1}|_{\text{img}} = 28.5$ cm.

Figures 11(a)-(e) show the interference patterns for the double-slit placed, respectively, at the positions $z_{o1} = 31.0, 28.5, 24.2, 20.0$, and 10.6 cm, corresponding to the effective diffraction lengths $Z_{\text{eff}} = 2.0, 0, -5.7, -13.9$, and -42.0 cm. The experiment has verified that the position for the object to be imaged [Fig. 11(b)] is at $z_{o1} = 28.5$ cm, which is equal to the diffraction length of the reference arm \bar{Z} . The regions left and right of this position correspond to positive and negative diffraction behavior, respectively. However, for an

amplitude-modulated object, the same pattern is obtained for both positive and negative diffraction with equal magnitude of diffraction length.



Fig. 11. Experimentally observed 2D interference patterns in the scheme of Fig. 10. [(a)-(e)]: the double slit is placed at the positions of $z_{01} = 31.0, 28.5, 24.2, 20.0$, and 10.6 cm, respectively, where (b) is the image of the double slit (Zhang et al., 2009b).

We have learned in Section 2 that the effective diffraction length in the interferometric scheme of Fig. 2 can be either positive or negative depending on whether the reference arm is longer or shorter than the object arm. We see again the two kinds of diffraction occurring in the present setup. In particular, this scheme may be realized with a null effective diffraction length $Z_{\text{eff}} = 0$, which implies that phase sensitive imaging may be accomplished without using a conventional lens. This effect cannot occur in the coherent regime. Figure 12 compares the output patterns of the interferometer in the same configuration using spatially incoherent and coherent light, when the double-slit is placed at the position $z_{01} = 28.5$ cm. The images of the double-slit when the interferometer is illuminated by the extended Na lamp are shown in the left column. After we insert a pinhole in front of the lamp to improve the spatial coherence, as expected, instead of obtaining an image we observe interference fringes, as shown in the right column of Fig. 12. In this case, lensless imaging cannot occur no matter where the object is placed.

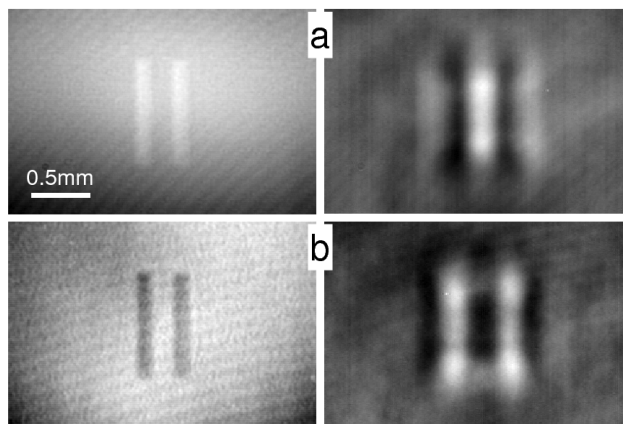


Fig. 12. Experimentally observed 2D patterns when a double-slit object is placed at the position $z_{01} = \bar{Z} = 28.5$ cm. Left column: image patterns when the source is spatially incoherent; right column: fringe patterns when the source is spatially coherent (with a pinhole aperture in front of the source). Figure (a) was recorded by CCD_1 and (b) by CCD_2 (Zhang et al., 2009b).

A negative diffraction length in wave propagation means phase-reversal diffraction of the wave-front. Recent research on electromagnetic metamaterials shows that negative refractive index materials may be engineered. When an electromagnetic wave travels in a negatively refracting medium, its wave-front undergoes phase-reversal diffraction (Pendry, 2008), thus a slab of negative refraction material can play the same role as a curved lens to perform imaging. Interestingly, the two different physical systems, incoherent interferometry and negative refraction material, reveal some similarity in phase-reversal diffraction (Zhang et al., 2009b).

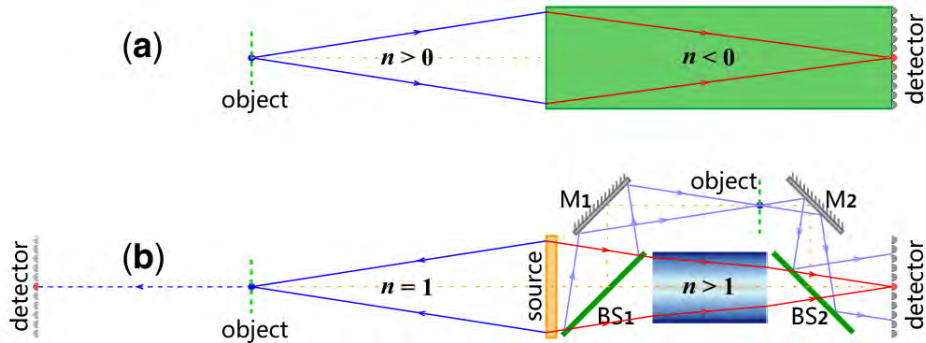


Fig. 13. Illustration of lensless imaging by two schemes. (a) Via successive diffraction through two media, where one is a negative refractive index medium. (b) Using an incoherent light interferometer; when the interferometer is opened out and the two arms are set along a line, the joint diffraction through them is comparable with that in (a) (Zhang et al., 2009b).

Figure 13 explains the similarity of the two models. In Fig. 13(a), we consider the successive diffraction of an object through two media, a positive refraction medium of length l_1 and index $n_1 > 0$ followed by a negative one of length l_2 and index $n_2 < 0$. Let $T(x_0)$ describe a

transmittance object, illuminated by a plane wave E_0 , then the output field after diffraction is written as

$$E(x) = E_0 \int T(x_0)H(x, x_0; n_1 l_1 + n_2 l_2, l_1/n_1 + l_2/n_2)dx_0. \quad (33)$$

When the net diffraction length in the successive propagation is null, i.e. $l_1/n_1 + l_2/n_2 = 0$, then $H(x, x_0; n_1 l_1 + n_2 l_2, 0) = \exp[i k_0(n_1 l_1 + n_2 l_2)] \delta(x - x_0)$ and we have

$$E(x) = E_0 \exp[i k_0(n_1 l_1 + n_2 l_2)] T(x). \quad (34)$$

Otherwise, Eq. (33) represents Fresnel diffraction with a diffraction length of $l_1/n_1 + l_2/n_2$

$$E(x) \propto E_0 \exp[i k_0(n_1 l_1 + n_2 l_2)] \int T(x_0)G(x - x_0, l_1/n_1 + l_2/n_2)dx_0, \quad (35)$$

which has the same form as Eq. (27)

To better compare the two schemes, in Fig. 13(b), the interferometer is opened out and the two arms are set along a line. We can see that the joint diffraction through the two arms is comparable with the geometry in Fig. 13(a).

Recently, various approaches for invisibility cloaking and transformation optics in complementary media with positive and negative refraction materials have been proposed, which can in theory accomplish exact optical cancellation between the object and its counterpart (Lai et al., 2009a, 2009b). In light of the similarity of time-reversal diffraction between incoherent interferometry and negatively refracting media, using the present scheme, we have conducted proof-of-principle experimental demonstrations of the theoretical proposals (Zhang et al., 2010; Gan et al., 2011). The physical analogue between the two different systems may provide a convenient research platform. Moreover, a form of nonlocal imaging as well as interference effects that were previously regarded as the signature of two-photon entanglement or intensity correlation of thermal light can now be realized in incoherent interferometry, which is associated with the first-order field correlation (Gao et al., 2009; Gan et al. 2009).

4. Conclusion

Interference effects in incoherent interferometry show different physics from that in coherent interferometry. In the latter case, two interfering fields have well-defined spatial distributions, whereas in the former case, these fields fluctuate randomly in space and the interference pattern appears only in the statistical average. Furthermore, incoherent interference relies entirely on the first-order spatial correlation of the two fields, so the object information is contained in the joint diffraction of the two fields. For certain optical geometries, phase reversal diffraction can occur through the first-order spatial correlation of incoherent light, thus providing a method of wave-front recovery without using a lens, and also a means for optical transformation.

Incoherent interferometry as a novel interference mechanism exhibits richer phenomena than the coherent type. Since it is not dependent on spatial coherence, the present method may find potential application in holography and other interference technologies, especially in those areas where a coherent source is unavailable. Incoherent holographic interferometry is fundamentally different from the previously known incoherent holography, while it can play the same role as coherent holography.

5. Acknowledgment

The authors thank L. A. Wu for helpful discussions. This work was supported by the National High Technology Research and Development Program of China, Project No. 2011AA120102 and the National Natural Science Foundation of China, Project No. 10874019.

6. References

- Cochran, G. (1966). New method of making Fresnel transforms with incoherent light. *J. Opt. Soc. Am.*, Vol.56, No.11, (November 1966) pp.1513-1517.
- Gabor, D. (1972). Holography, 1948-1971, *Science*, New Series, Vol.177, No.4046, (July 1972) pp. 299-313.
- Gan, Sh., Zhang, S. H., Xiong, J., & Wang, K., (2009). Interference from a nonlocal double-slit through one-photon process, *Optics Express* Vol.17, No.26, (December 2009) pp.23672-23677.
- Gan, Sh., Zhang, S. H., Zhao, T., Xiong, J., Zhang, X., & Wang K., (2011). Cloaking of a phase object in ghost imaging, *Appl. Phys. Letts.* Vol.98, No.11, (March 2011) 111102, ISSN 0003-6951.
- Gao, L., Zhang, S. H., Xiong, J., Gan, Sh., Feng, L. J., Cao, D. Zh., & Wang, K., (2009). Correlated imaging with one-photon interference, *Phys. Rev. A* Vol.80, No.2, (August 2009) 021806(R), ISSN 1050-2947.
- Goodman, J. W. (1996). *Introduction to Fourier Optics* (Second Edition), p.371, The McGraw-Hill Companies, Inc. New York.
- Lai, Y., Chen, H. Y., Zhang, Zh. Q., & Chan, C. T., (2009a). Complementary media invisibility cloak that cloaks objects at a distance outside the cloaking shell, *Phys. Rev. Lett.* Vol.102, No.9, (March 2009) 093901, ISSN 0031-9007.
- Lai, Y., Ng, J., Chen, H. Y., Han, D. Zh., Xiao, J. J., Zhang, Zh. Q., & Chan, C. T., (2009b). Illusion optics: the optical transformation of an object into another object, *Phys. Rev. Lett.* Vol.102, No.25, (June 2009) 253902, ISSN 0031-9007.
- Lohmann, A. W. (1965). Wavefront reconstruction for incoherent objects. *J. Opt. Soc. Am.*, Vol.55, Issue 11, (November 1965) pp. 1555-1556.
- Mertz, L. & Young, N. O. (1963). Fresnel transformations of images, In: *Proceedings of the Conference on Optical Instruments and Techniques*, K.J. Habell, (Ed.), p. 305, John Wiley and Sons, New York, NY.
- Pendry, J. B. (2008). Time reversal and negative refraction. *Science* Vol.322, (October 2008) pp. 71-73, ISSN 1095-9203.
- Stroke, G. W. & Restrick, R. C. (1965). Holography with spatially noncoherent light. *Appl. Phys. Lett.*, Vol.7, Issue 9, (November 1965) pp.229-231, ISSN 0003-6951.
- Zhang, S. H., (July 2010). The first-order field correlation effects of spatially incoherent light, In: *PhD thesis, Beijing Normal University*, Wang, K. (Dir), Available from: <http://d.wanfangdata.com.cn/Thesis_Y1776851.aspx>.
- Zhang, S. H., Gao L., Xiong, J., Feng, L. J., Cao, D. Zh., & Wang, K., (2009a). Spatial Interference: From Coherent to Incoherent, *Phys. Rev. Lett.* Vol.102, No.7 (February 2009) 073904, ISSN 0031-9007.

Zhang, S. H., Gan, Sh., Cao, D. Zh., Xiong, J., Zhang X., & Wang, K., (2009b). Phase-reversal diffraction in incoherent light, *Phys. Rev. A* Vol.80, No.3, (September 2009) 031895(R), ISSN 1050-2947.

Zhang, S. H., Gan, Sh., Xiong, J., Zhang, X., & Wang, K., (2010). Illusion optics in chaotic light, *Phys. Rev. A* Vol.82, No.2, (August 2010) 021804(R), ISSN 1050-2947.